iScience

CellPress
OPEN ACCESS

Article

Prenatal alcohol alters inflammatory signatures in enteric portal tissues following adult-onset cerebrovascular ischemic stroke

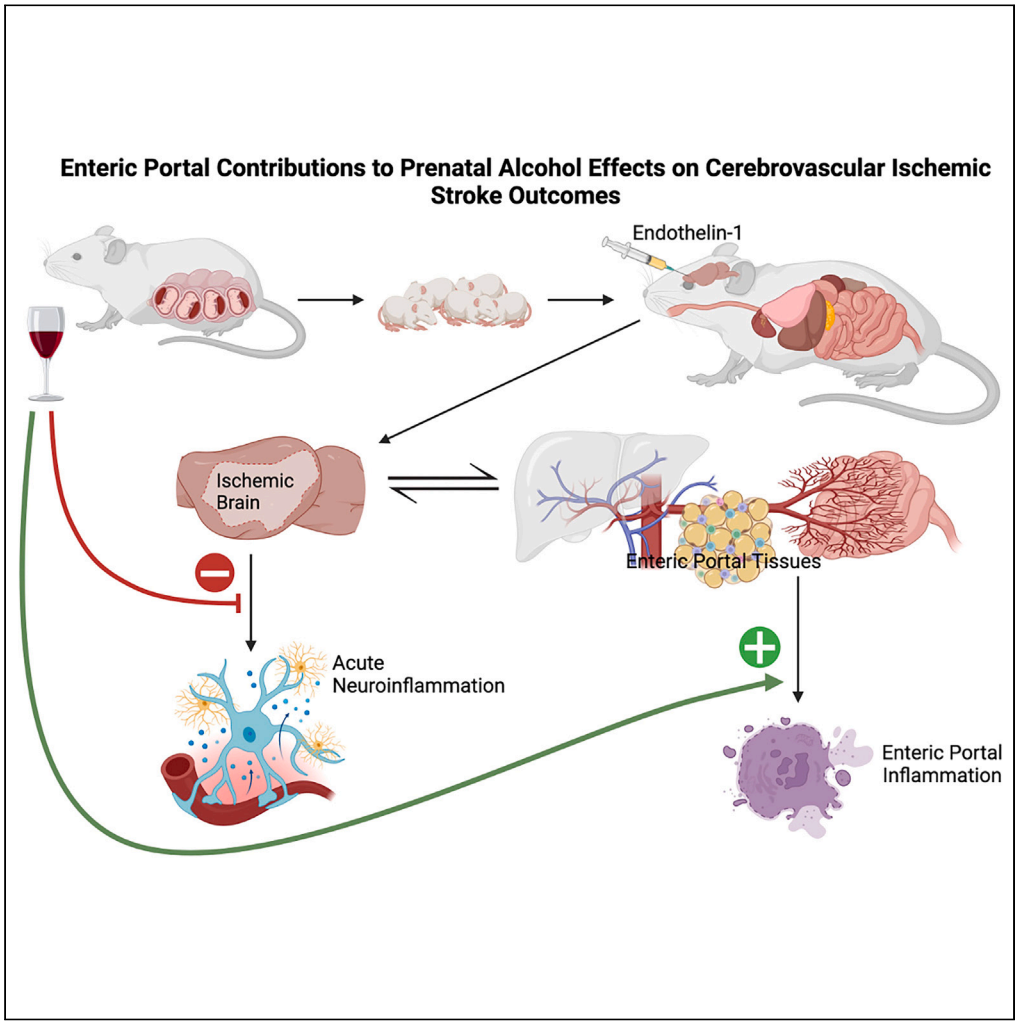

Marisa R. Pinson, Shameena Bake, David A. Hurst, Nadia T. Samiya, Farida Sohrabji, Rajesh C. Miranda

rmiranda@tamu.edu

Highlights

Prenatal alcohol exposure (PAE) exacerbates effects of acute adult-onset disease

PAE promotes basal inflammatory necroptosis in adult liver

PAE inhibits brain cytokine response to cerebrovascular ischemic stroke in adults

PAE elevates inflammatory gene networks in enteric portal tissues after stroke

Pinson et al., iScience 26, 107920
October 20, 2023
https://doi.org/10.1016/j.isci.2023.107920

iScience

CellPress
OPEN ACCESS

Article

Prenatal alcohol alters inflammatory signatures in enteric portal tissues following adult-onset cerebrovascular ischemic stroke

Marisa R. Pinson,[1,4] Shameena Bake,[1,2,4] David A. Hurst,[1] Nadia T. Samiya,[1] Farida Sohrabji,[1,2,3] and Rajesh C. Miranda[1,2,3,5,*]

SUMMARY

Prenatal alcohol exposure (PAE) impairs recovery from cerebrovascular ischemic stroke in adult rodents. Since the gut becomes dysbiotic following stroke, we assessed links between PAE and enteric portal inflammation. Adult control and PAE rat offspring received a unilateral endothelin-1-induced occlusion of the middle cerebral artery. Post-stroke behavioral disabilities and brain cytokines were assessed. Mesenteric adipose and liver transcriptomes were assessed from stroke-exposed and stroke-naive offspring. We identified, in the liver of stroke-naive animals, a moderate correlation between PAE and a gene network for inflammatory necroptosis. PAE inhibited the acute-phase brain inflammatory cytokine response to stroke. Post-stroke neurological function was correlated with an adipose gene network associated with B-lymphocyte differentiation and nuclear factor κB (NF-κB) signaling and with a liver pro-inflammatory gene network. Collectively, PAE inhibits brain inflammation but results in an inflammatory signature in enteric portal tissues after stroke, suggesting that PAE persistently and adversely impacts the gut-brain axis following adult-onset disease.

INTRODUCTION

Prenatal stressors, such as prenatal alcohol exposure (PAE), have detrimental impacts on the development of the fetus, contributing to elevated risk for cardiovascular, metabolic, and other diseases later in life.[1–3] Specifically, PAE occurs in ~8%–15% of births in North America,[4–6] with prevalence of fetal alcohol spectrum disorder (FASD) in 1.1%–9.8% of the school-age population in the US,[7,8] making PAE the largest single cause of neurodevelopment disabilities and growth deficits. While historically studies have primarily focused on brain-based disabilities,[9] there is growing recognition that FASD is a "whole-body" diagnosis with an increased risk for developing diseases beyond the brain (e.g., cardiovascular, endocrine/metabolic, and other physiological systems) that persists throughout the lifespan.[10,11] Moreover, there is a markedly higher mortality rate among the FASD population, with a rapid increase starting in early adolescence/young adulthood,[12] highlighting the importance for a better understanding of the systemic effects of PAE on adult health and resilience in response to an adult-onset health crisis such as cerebrovascular ischemic stroke.

A hypertensive phenotype has been characterized in rodent models, with PAE contributing to increased peripheral arterial pressure[13] and increased cranially directed blood flow in carotid arteries[14] in adult offspring. These findings are consistent with more recent human studies showing that children and teenagers with a diagnosis of fetal alcohol syndrome (FAS) or partial FAS were 8.46-fold more likely to also be diagnosed with hypertension,[15] an important risk factor for stroke.[16] Additional risk factors for stroke have been documented as a consequence of PAE, including impaired glucose metabolism,[17] insulin resistance,[18] and renal dysfunction.[13] Moreover, we have previously shown in both mouse and rat models that adult PAE offspring exhibit impaired neurobehavioral recovery after stroke.[14,19] Altogether, this suggests that vulnerability to cerebrovascular ischemic stroke may emerge early in FASD populations and that resilience to such an adverse health event is impaired after PAE. However, the underlying etiology for this impaired response and recovery remains to be investigated.

One potential avenue for investigation is the gut-brain axis, which has been documented to play an important role in stroke outcomes. After stroke, the gut rapidly becomes "leaky", allowing intestinal and microbial products to escape into circulation.[20–22] These products are directly transported to mesenteric adipose tissue, and subsequently to the liver via portal circulation, potentially influencing the physiology of both organs (reviewed in Konrad et al[23]). Moreover, previous work identified the importance of cytokines of the mesenteric adipose and liver in profiling differences in young adult PAE offspring, with specific cytokines aiding in prediction of physiological and behavioral

[1]Department of Neuroscience and Experimental Therapeutics, Texas A&M School of Medicine, Bryan, TX, USA
[2]Women's Health in Neuroscience Program, Texas A&M University School of Medicine, Bryan, TX, USA
[3]Senior author
[4]These authors contributed equally
[5]Lead contact
*Correspondence: rmiranda@tamu.edu
https://doi.org/10.1016/j.isci.2023.107920

outcomes.[17] This suggests that underlying changes in the mesenteric adipose tissue and liver may influence resilience to stroke, contributing to impaired recovery.

To examine this relationship, we conducted bulk RNA sequencing (RNA-seq) analyses on mesenteric adipose tissue and liver from adult rats using a 2 x 2 factorial study design which included prenatal treatment (unexposed controls and PAE offspring) and adult stroke exposure (stroke-naive adult rats and animals that received a unilateral cerebrovascular ischemic stroke) as independent variables, to assess the interaction between prenatal history and adult-onset disease on gene expression. For this study, we also used samples from animals characterized behaviorally and metabolically in previous studies,[17,19] to build multivariable datasets, to identify significant associations between gene expression changes in enteric portal tissue efferents and neurological and behavioral outcomes. Differential gene expression analyses found enhanced alteration in transcriptomic adaptations in response to stroke because of PAE. Pathway analysis of this enhanced response identified a heightened pro-inflammatory response of the mesenteric adipose with a weakened anti-inflammatory response in the liver of young adult PAE rats that also experienced an ischemic stroke.

RESULTS

Effect of ischemic stroke and PAE on brain cytokines

Stroke elevates brain cytokines in the ischemic hemisphere

We assessed the levels of a panel of cytokines in the ischemic and contralateral (non-ischemic) hemispheres at 48 h following the stroke episode. All samples were from animals in our previous study that showed 5–6 month-old adult PAE rats experienced worse recovery from stroke.[19] Multivariate analysis showed that there was a global, statistically significant increase in the expression of cytokines measured in the ischemic hemisphere compared to the contralateral non-ischemic hemisphere (multivariate analysis of variance [MANOVA], Pillai's Trace Statistic, $F(1,48) = 64.97$, $p < 0.00001$). Post hoc ANOVA verified that a majority of assessed cytokines (granulocyte colony-stimulating factor [G-CSF], Eotaxin, granulocyte-macrophage colony-stimulating factor [GM-CSF], interleukin-1-alpha [IL1-alpha], Leptin, macrophage inflammatory protein 1-alpha [MIP-1-alpha], IL-4, IL1-beta, IL-2, IL-6, epidermal growth factor [EGF], IL-13, IL-10, IL12-P70, interferon [IFN]-gamma, IL-5, IL-17A, IL-18, monocyte chemoattractant protein-1 [MCP-1], interferon gamma-induced protein 10 [IP-10], vascular endothelial growth factor [VEGF], Fractalkine, lipopolysaccharide-induced CXC chemokine [LIX], MIP2, tumor necrosis factor alpha [TNF-alpha]) were significantly elevated in the ischemic stroke hemisphere compared to the non-ischemic hemisphere (all $F(1,51)>5.97$, all p values <0.018) with the exception of growth related oncogene-keratinocyte chemoattractant/CXCL1 (GRO-KC) and Regulated upon Activation, Normal T cell Expressed and Presumably Secreted/CCL5 [RANTES] which were not significantly increased. In the same MANOVA model, neither offspring sex nor prenatal treatment had a global effect on cytokine expression ($p = 0.481$ and $p = 0.212$ for sex and prenatal exposure, respectively).

PAE inhibits the cytokine response to stroke

Since ischemic stroke itself resulted in significant global increase in cytokines, we computed the ratio of cytokine expression in the ischemic hemisphere relative to the non-ischemic hemisphere and then computed ANOVAs for the main effects of prenatal exposure and sex. There were no significant main effects of sex for all of the assessed cytokines. However, the ischemic to non-ischemic ratio of several cytokines were significantly decreased by PAE (Figure 1). These included Eotaxin ($F(1,23) = 8.75$, $p = 0.0071$), GM-CSF ($F(1,23) = 11.2$, $p = 0.0028$), IL-4 ($F(1,23) = 10.42$, $p = 0.0037$), IL-1-beta ($F(1,23) = 8.57$, $p = 0.0076$), IL-13 ($F(1,23) = 5.3$, $p = 0.031$), IL-10 ($F(1,23) = 6.24$, $p = 0.02$), IL-12-P70 ($F(1,31) = 4.64$, $p = 0.042$), IL-5 ($F(1,23) = 4.11$, $p = 0.054$), LIX ($F(1,31) = 7.81$, $p = 0.01$), and RANTES ($F(1,31) = 4.78$, $p = 0.039$). We next conducted a series of multivariate analyses to identify a combination of cytokines that collectively explained the suppressive effects of PAE on the brain cytokine response to ischemia. The best multivariate outcome (Pillai's Trace Statistic, $F(1,23) = 5.82$, $p = 0.0082$) included a combination of the cytokines G-CSF, Eotaxin, GM-CSF, IL1-alpha, Leptin, IL-4, IL1-beta, IL-2, IL-6, IL-13, IL-10, IL12-P70, IL-5, MIP2, LIX, and TNF-alpha.

RNA-seq analysis of PAE effects on enteric portal efferent tissues in naive adults and following ischemic stroke

PAE activates TCA cycle while suppressing rRNA processing in the mesenteric adipose in healthy adult rats

Adults with FASD report increased gastrointestinal (e.g., irritable bowel syndrome, chronic diarrhea) and metabolic dysregulation.[11] Thus, we wanted to determine the long-term consequences of PAE on the transcriptome of the mesenteric adipose of healthy young adult (5 months) male and female offspring. We conducted bulk RNA-seq (males n = 3/control and n = 4/PAE, females n = 4/control and n = 4/PAE). RNA-seq analysis identified 19 significantly differentially expressed genes (DEGs; false discovery rate [FDR]-corrected $p < 0.05$), including 2 downregulated genes (10.53%) and 17 upregulated genes (89.47%) (Figure 2A; Table S1). While separate analyses of just male and female animals identified DEGs specific to each sex in the mesenteric adipose (Figure S2A; Table S2 for Males; Table S3 for Females), the present study focused on downstream analyses of the PAE-dependent, sex-independent DEGs to characterize the overarching effects of PAE.

Pathway analysis using the 19 PAE-dependent DEGs did not identify a previously known enriched pathway. All animals included in this study were healthy as assessed by veterinarian monitoring, having only been exposed to ethanol 5 months prior *in utero*, and housed in the same environment which minimized external stressors. As predicted therefore, persistent transcriptomic differences in adulthood due to PAE were small, at least when using strict, FDR-limited parametric criteria. Therefore, we expanded our inclusion criteria to capture more subtle differences. For this secondary analysis, differentially regulated genes (DRGs) were defined by meeting all three of the following

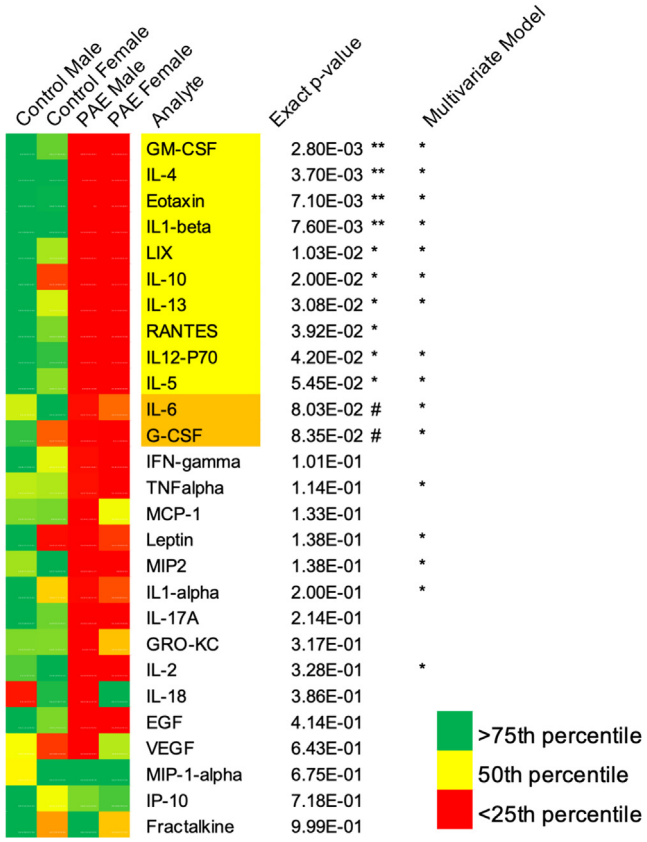

Figure 1. PAE inhibits expression of brain cytokines following stroke

Heatmap shows the ratio of cytokines in the ischemic hemisphere relative to the expression in the contralateral, non-ischemic hemisphere in control and PAE male and female offspring. There was no main effect of significant effect of offspring sex in either multivariate (MANOVA) or univariate (ANOVA) models. ANOVA models showed a significant main effect of prenatal exposure for 10 cytokines (asterisks) and a marginal effect for an additional two cytokines (#). The best multivariate model (Pillai's Trace Statistic, $F(1,23) = 5.82$, $p = 0.0082$), created by sequentially adding and subtracting cytokines from the model indicated that 16 cytokines (asterisks), including some that were by themselves not significant by univariate analysis contributed overall to a significant treatment effect of PAE on the suppression of the brain cytokine response to ischemic stroke. Green indicates expression ratio >75th percentile, yellow, at 50th percentile and red, <25th percentile, in the ischemic hemisphere compared to the non-ischemic contralateral hemisphere.

independent criteria: (1) unadjusted p value<0.05, (2) large effect size (Hedge's g > 0.8), and (3) nonoverlapping 95% confidence intervals around the mean of each treatment group. This reanalysis identified 452 genes that met criterion, 129 downregulated, and 323 upregulated (Table S4). Pathway analysis conducted on this expanded gene list using *ReactomePA* identified upregulation of tricarboxylic acid (TCA) cycle-associated genes and a downregulation of rRNA processing-associated genes (Figure 2B).

Next, we sought to identify mesenteric adipose gene networks that might be enriched for DRGs. Using weighted gene co-expression network analysis (WGCNA), we identified 34 modules of gene networks (Table S5). Approximately 74% (25 out of 34) of these modules contained at least one DRG (Figure S3). The module with the highest enrichment score for DRGs within mesenteric adipose was the *pink* module (0.13 enrichment score, 149 DRGs/1,132 module genes; Figure S3). Kyoto Encyclopedia of Genes and Genomes (KEGG) analysis of the *pink* module identified upregulation of integral enzymes of the TCA cycle (adjusted p = 0.032; Figure S4A), in concordance with the DRG pathway analysis (Figure 2B).

PAE dysregulates necroptosis in the liver in healthy young adult rats

The enteric portal system carries blood from the intestines through mesenteric adipose tissue to the liver. Portal circulation contributes approximately 70% of the hepatic blood supply, making the liver an important efferent target that is sensitive to physiologic adaptations in both intestines and mesenteric adipose. Therefore, as with mesenteric adipose tissue, we assessed the long-term consequences of PAE on the transcriptome of the liver of healthy young adult males and females (5 months; males n = 3/control and n = 4/PAE, females n = 4/control and n = 4/PAE). RNA-seq analysis identified 5 significantly DEGs (FDR-corrected $p < 0.05$), all of which were upregulated (Figure 3; Table S6). While separate analyses of male and female animals identified DEGs specific to each sex in the liver (Figure S2B; Table S7 for Males; Table S8 for Females), the present study focused on downstream analyses of the PAE-dependent, sex-independent DEGs to characterize the overarching effects of PAE.

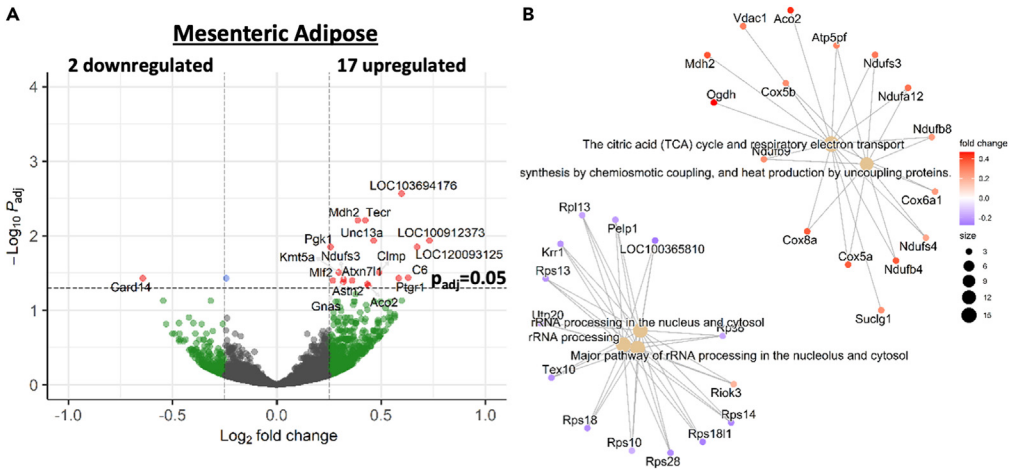

Figure 2. PAE has moderate effects on the mesenteric adipose tissue of healthy young adult rats

(A) Volcano plot of log2 fold change and −log10 adjusted p value of all genes differentially expressed (DEGs) in mesenteric adipose of control vs. PAE 5 months old rats.

(B) Enrichment plots depicting linkages between PAE-sensitive DRGs and biological pathways. Figure was created using ReactomePA. Control stroke-naive male n = 3, Control stroke-naive female n = 4, PAE stroke-naive male n = 4, PAE stroke-naive female n = 4.

Pathway analysis using these 5 DEGs did not identify an enriched pathway. Therefore, we adopted the approach for secondary reanalysis that we used for the mesenteric adipose, to gain a more nuanced understanding of underlying differences in the liver transcriptomes between control and PAE young adult rats. This reanalysis identified 192 DRGs (90 downregulated, 101 upregulated; Table S9) using the same criteria defined earlier. However, pathway analysis conducted on this expanded gene list used *ReactomePA*, which was again unable to identify an enrichment of any known pathway.

Next, we sought to identify hepatic gene networks that might be enriched for DRGs. Using WGCNA, we identified 27 modules of gene networks (Table S10). Approximately 85% (23 of these 27) of identified modules contained at least one DRG (Figure S5). The module with the highest enrichment score for DRGs of the liver was the *royalblue* module (0.04 enrichment, 9 DRGs/242 module genes; Figure S5). Gene ontology (GO) analysis of the *royalblue* module identified necroptotic process (adjusted p = 0.026, 5/34 GO genes, GO:0070266) as potentially dysregulated.

PAE alters transcriptomic response to stroke in mesenteric adipose and liver

To compare how PAE young adult rats respond to a systemic health stressor differently than control animals, we compared the stroke-naive animals characterized earlier to littermates of the same age (5 months) that had received middle cerebral artery occlusion (MCAo) 2 days prior. Samples were from animals in our previous study that showed young adult PAE rats experienced worse recovery post-stroke.[19] The analyses discussed below focus on PAE-dependent, sex-independent DEGs to characterize the overarching effects of PAE, but we did observe stroke-sensitive DEGs unique to males and females of both controls and PAE animals in mesenteric adipose and the liver (Figure S6; Tables S11, S12, S13, S14, S15, S16, S17, and S18) that are worthy of consideration in future studies.

Mesenteric adipose tissue. Bulk RNA-seq was conducted on the mesenteric adipose of stroke-naive and stroke animals, for control (males n = 3/stroke-naive and n = 3/stroke, females n = 4/stroke-naive and n = 4/stroke) and for PAE (males n = 4/stroke-naive and n = 4/stroke, females n = 4/stroke-naive and n = 4/stroke). RNA-seq analysis of control stroke-naive v. stroke identified 1,465 significant DEGs (FDR-corrected $p < 0.05$), including 509 downregulated genes (34.74%) and 956 upregulated genes (65.26%) (Figure 4A; Table S19). Analysis of PAE stroke-naive v. stroke identified 1,653 significant DEGs (FDR-corrected $p < 0.05$), including 703 down-regulated genes (42.52%) and 950 up-regulated genes (57.47%) (Figure 4B; Table S20). Thus, there were similar levels of upregulated stroke-sensitive DEGs (956 in control v. 950 in PAE) and similar levels of downregulated stroke-sensitive DEGs (509 in control v. 703 in PAE) following stroke. To determine how similar the transcriptomic responses in the mesenteric adipose were between control and PAE offspring, stroke-sensitive DEGs were compared between the groups. This analysis showed that 1,243 stroke-sensitive DEGs were unique to PAE while 1,055 stroke-sensitive DEGs were unique to control, with only 410 stroke-sensitive DEGs being common between the groups (Figure 4C). These data show that PAE status was an important determinant of the adult mesenteric adipose response to stroke.

Liver. Additionally, bulk RNA-seq was conducted on the liver of stroke-naive and stroke animals, for control (males n = 3/stroke-naive and n = 3/stroke, females n = 4/stroke-naive and n = 4/stroke) and for PAE (males n = 4/stroke-naive and n = 4/stroke, females n = 4/stroke-naive and n = 4/stroke). RNA-seq analysis of control stroke-naive v. stroke identified 761 significant DEGs (FDR-corrected $p < 0.05$), including 256

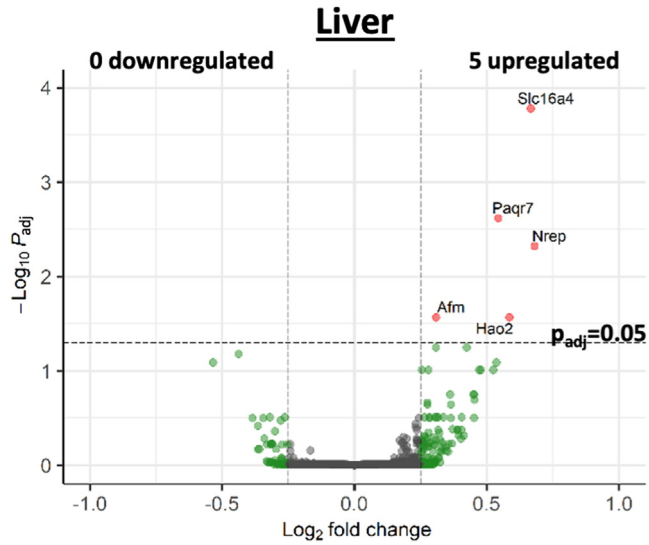

Figure 3. PAE has moderate effects on the liver of healthy young adult rats

Volcano plot of log2 fold change and −log10 adjusted p value of all genes differentially expressed (DEGs) in mesenteric adipose of control vs. PAE 5 months old rats. Control stroke-naive male n = 3, Control stroke-naive female n = 4, PAE stroke-naive male n = 4, PAE stroke-naive female n = 4.

downregulated genes (33.64%) and 505 upregulated genes (66.36%) (Figure 4D; Table S21). Analysis of PAE stroke-naive v. stroke identified 1,447 significant DEGs (FDR-corrected $p < 0.05$), including 612 downregulated genes (42.29%) and 835 upregulated genes (57.71%) (Figure 4E; Table S22). This showed greater transcriptomic dysregulation in the liver compared to mesenteric adipose as there was a 1.6-fold increase in upregulated stroke-sensitive DEGs (505 in control v. 835 in PAE) and a 2.4-fold increase in downregulated stroke-sensitive DEGs (256 in control v. 612 in PAE) following stroke, compared to control offspring. To determine the extent of similarity in the transcriptomic responses in the liver between control and PAE, stroke-sensitive DEGs were compared between the groups. 999 stroke-sensitive DEGs were unique to PAE while 313 stroke-sensitive DEGs were unique to control, with only 448 stroke-sensitive DEGs being common between the groups (Figure 4F). These data show that, as with mesenteric adipose tissue, PAE status was an important determinant of the adult hepatic response to cerebrovascular stroke.

We further conducted qRT-PCR of selected transcripts with moderate- to high-abundance sequence reads that were also differentially regulated by RNA-seq analysis, focusing our analysis on intron-spanning exons at the 5′ end of target mRNAs. This 5′-biased qRT-PCR analysis replicated RNA-seq outcomes at very large qRT-PCR effect size changes (Hedges 'g' >1.0, Figure S7) suggesting either that qRT-PCR is not as sensitive to changes in gene expression or that 5′-biased amplicons only partly reflect all gene changes visualizable by sequence analysis, particularly at smaller effect sizes. We also noted that selected transcripts encoded within unannotated loci in the rat genome were significantly induced in either control or PAE animals after stroke. Some, like LOC103694395, were putative long non-protein-coding RNAs (lncRNAs), but not evolutionarily conserved, with no known orthologs or paralogs in other species (mapped using the University of California Santa Cruz [UCSC] genome browser, https://genome.ucsc.edu/, Rat assembly mRatBN7.2/rn), and are presumptive rat-specific hepatic lncRNA adaptations to stroke. Other unannotated transcripts did exhibit evolutionary conservation but, as with LOC102552988, were predicted to encode an integral membrane protein, highly expressed in the liver, but of unknown function (https://www.ncbi.nlm.nih.gov/gene/102552988). Consequently, transcripts encoded by unannotated loci were eliminated from further analysis.

Control mesenteric adipose responds to stroke by activating TCA cycle while PAE mesenteric adipose responds by upregulating cell cycle-associated genes

Pathway analysis utilizing *ReactomePA* was conducted separately on those stroke-sensitive DEGs that were unique to control and to PAE in mesenteric adipose. For stroke-sensitive DEGs unique to control, pathways associated with the TCA cycle, gluconeogenesis, fatty acid metabolism, and other pathways associated with energy production were significantly overrepresented and overall upregulated (Figure 5A). Because TCA cycle was identified earlier as PAE-sensitive in mesenteric adipose of stroke-naive animals (Figure S4A), we conducted KEGG analysis of stroke-sensitive DEGs unique to control and found that similar integral members of the TCA cycle were upregulated (adjusted $p < 0.0001$; Figure S4B). For stroke-sensitive DEGs unique to PAE, pathways associated with the cell cycle regulation and progression were significantly overrepresented and overall upregulated (Figure 5B). Interestingly, genes for histones and histone-like transcripts were consistent across all the identified pathways.

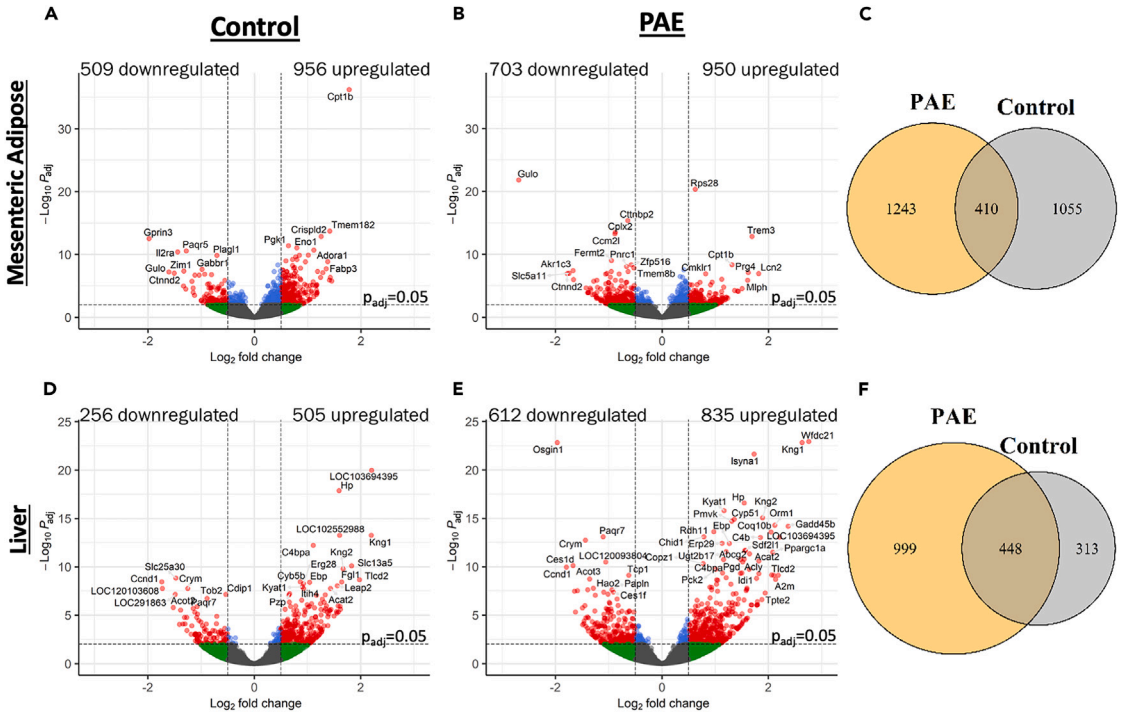

Figure 4. PAE results in altered response to cerebrovascular stroke in mesenteric adipose tissue and liver

(A–E) Volcano plots of log2 fold change and −log10 adjusted p value of all DEGs in mesenteric adipose tissue of Control (A) and PAE (B) offspring following cerebrovascular ischemic stroke. (C) Venn diagram comparing DEGs in mesenteric adipose tissue. Volcano plots of log2 fold change and −log10 adjusted p value of all DEGs in liver of Control (D) and PAE (E) offspring following cerebrovascular ischemic stroke.

(F) Venn diagram comparing DEGs in liver. Control: stroke-naive male = 3, stroke-naive female = 4, stroke male = 3, stroke female = 4. PAE: stroke-naive male = 4, stroke-naive female = 4, stroke male = 4, stroke female = 4.

PAE liver responds to stroke by upregulating cholesterol synthesis

Pathway analysis utilizing *ReactomePA* was conducted separately on those stroke-sensitive DEGs that were unique to control and to PAE in the liver. For stroke-sensitive DEGs unique to control, no known pathways were identified. For stroke-sensitive DEGs unique to PAE, pathways associated with metabolism of steroids and cholesterol biosynthesis were significantly overrepresented and overall upregulated while triglyceride metabolism was significantly overrepresented but had both upregulated and downregulated genes (Figure 6).

WGCNA analysis reveals gene networks in mesenteric adipose and liver that are correlated with worse stroke outcomes

Because we previously showed that PAE resulted in a worse neurological scores post-stroke,[19] we conducted a correlation analysis between WGCNA module eigengenes (MEs) and neurological score to identify gene networks of the mesenteric adipose and liver (Figures S8A and S8B, respectively) that were sensitive to stroke. WGCNA module construction included samples only from stroke animals (control and PAE), and modules were constructed separately for mesenteric adipose and liver.

In the mesenteric adipose, we identified statistically significant relationships between neural score and the adipose *darkgreen* (Pearson's r = 0.518, p = 0.048) and *green* (Pearson's r = −0.608, p = 0.0161) MEs (Figure S8A). Gene ontology of the *darkgreen* module identified B-lymphocyte differentiation and NFκ-B signaling (Figure 7A) while gene ontology of the *green* module identified mitochondrial transcription, fatty acid biosynthetic process, and memory T cell differentiation (Figure 7B) as cellular processes that were statistically overrepresented.

In the liver, we identified statistically significant relationships between neural score and the hepatic *darkgreen* ME (Pearson's r = −0.629, p = 0.012; Figure S8B). Gene ontology of the hepatic *darkgreen* module identified negative regulation of interleukin-13/5/4 production and lipid/fatty acid metabolic processes (Figure 7C) as cellular functions that were statistically overrepresented.

Cytokines of the ischemic hemisphere correlate with different gene networks in control and PAE mesenteric adipose

Next, we assessed the extent to which changes in brain and plasma levels of cytokines were associated with the identified WGCNA gene networks in mesenteric adipose tissue. Therefore, we conducted correlation analyses between WGCNA modules and cytokine levels as well as hierarchical clustering analysis using Pearson correlation (Figure 8). Cytokines from the plasma, left brain hemisphere (ipsilateral to MCAo), and right brain hemisphere (contralateral to MCAo) were included in the analyses. Data for plasma cytokines were as previously

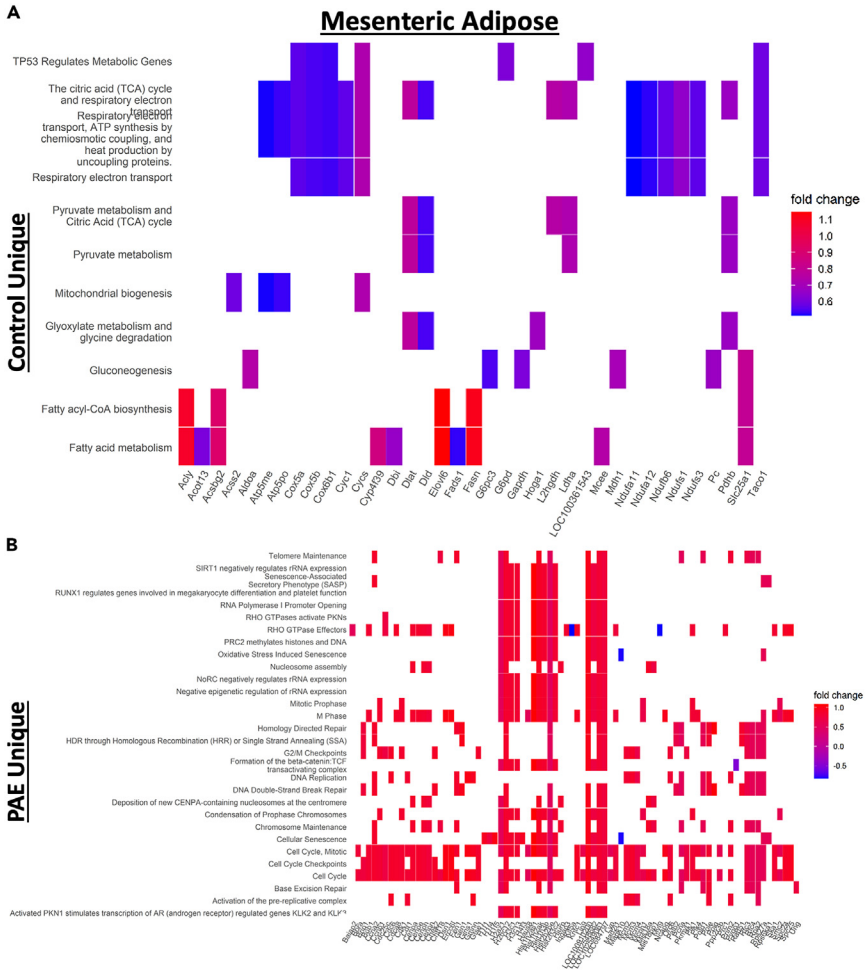

Figure 5. Different pathways are activated in mesenteric adipose tissue of control and PAE offspring post-stroke

(A) Heatmap depicting pathways enriched for DEGs unique to control response to stroke.

(B) Heatmap depicting pathways enriched for DEGs unique to PAE response to stroke. Figures were created using ReactomePA. Control: stroke-naive male = 3, stroke-naive female = 4, stroke male = 3, stroke female = 4. PAE: stroke-naive male = 4, stroke-naive female = 4, stroke male = 4, stroke female = 4.

published,[17] while data from brain cytokines were as reported earlier. Of interest was a clustering of left hemisphere (ipsilateral to MCAo) cytokines that had trending ($0.05 < p < 0.1$) to significant ($p < 0.05$) positive correlations with 4 WGCNA modules (*darkgreen, midnightblue, magenta, pink*) that also clustered together. This cluster of 4 WGCNA modules also subclustered (*darkgreen/midnightblue* v. *magenta/pink*), reflecting differing DEG enrichment scores that favored either PAE or control. Specifically, the *darkgreen* module was more highly enriched in PAE-unique DEGs while the *magenta* and *pink* modules were more highly enriched in control-unique DEGs (Table 1). For DEG enrichment scores of all modules of the mesenteric adipose please see Figure S9.

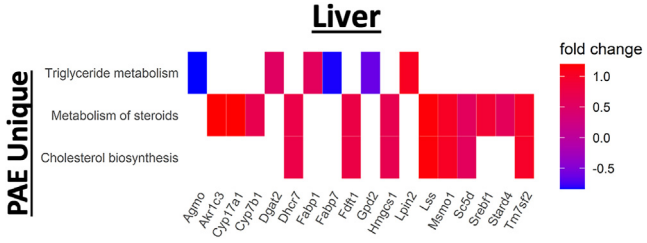

Figure 6. Unique pathways are activated in liver of PAE offspring post-stroke

Heatmap depicting pathways enriched for DEGs unique to PAE response to stroke. Figure was created using ReactomePA. PAE: stroke-naive male = 4, stroke-naive female = 4, stroke male = 4, stroke female = 4.

Figure 7. Gene networks linked to worse neural score in PAE offspring are enriched for pro-inflammatory pathways

(A–C) Gene ontology (GO) analysis of genes of the mesenteric adipose tissue modules *darkgreen* (A) and *green* (B) focused on biological processes. GO analysis of genes of the liver module *darkgreen* (C) focused on biological processes. Control stroke male n = 3, Control stroke female n = 4, PAE stroke male n = 4, PAE stroke female n = 4.

Gene ontology analysis was conducted on these 4 modules. The adipose *darkgreen* module was discussed earlier in regard to neural score post-stroke and was enriched for B-lymphocyte differentiation and NKκ-B signaling (Figure 7A). The adipose *midnightblue* module had DNA metabolism (Figure S10A) as statistically overrepresented. The adipose *magenta* module had an overrepresentation of genes associated with membrane fusion and response to doublestranded DNA (dsDNA) (Figure S10B) while the *pink* module had an overrepresentation of genes associated with pyrimidine metabolism, hematopoietic stem cell proliferation, and dendritic cell activation (Figure S10C).

Cytokine expression in the cerebral hemisphere ipsilateral to the stroke is correlated with the overlapping gene networks in control and PAE liver

As with the mesenteric adipose, we were interested in the relationship between cytokine levels and WGCNA gene networks identified in the liver and conducted similar analyses as those described earlier for adipose tissue (Figure 9). Of interest was a clustering of left hemisphere (ipsilateral to MCAo) cytokines that had trending to significant positive correlations with 4 WGCNA modules (*greenyellow, lightyellow, royalblue, tan*) that also clustered together. For all 4 of these WGCNA modules, enrichment for PAE-unique DEGs was higher compared to control-unique DEGs (Table 2), revealing a larger PAE response in these shared modules. For DEG enrichment scores of all modules of the liver please see Figure S11.

Gene ontology analysis was conducted on these 4 modules. Genes of the hepatic *greenyellow* module were associated with response to environmental stress and myeloid cell differentiation (Figure S12A). Genes of the hepatic *lightyellow* module were associated with heterochromatin organization and response to hormonal signaling (Figure S12B). Genes of the hepatic *royalblue* module were most highly associated with response to cortisol (Figure S12C). Genes of the hepatic *tan* module were most significant for an association with chemosensation (response to chemical stimuli/sensory perception; Figure S12D).

DISCUSSION

In this study, we report that prenatal alcohol exposure results in a global suppression of brain cytokines/chemokines which are normally elevated as an acute-phase injury response to stroke. Importantly, the majority of suppressed cytokines like IL-1α, IL-1β, IL-6, IL-12-P70,

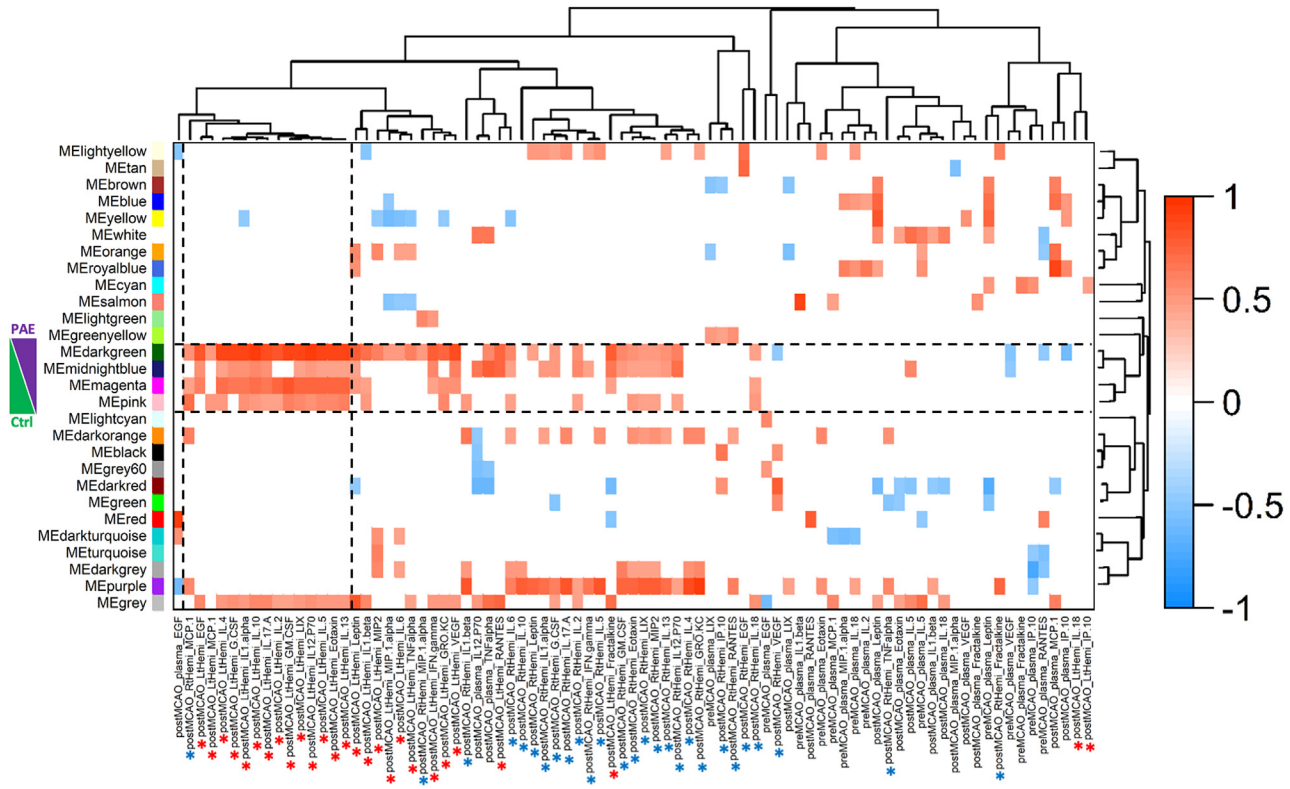

Figure 8. WGCNA reveals gene networks of the mesenteric adipose tissue associated with stroked-hemisphere cytokines

Heatmap of module-trait relationships depicting correlations between module eigengenes (ME) and fetal-placenta growth parameters. Only significant ($p < 0.05$) and trending ($0.05 < p < 0.1$) correlations are shown. The degree of correlation (r) is illustrated with the color legend. Red asterisks indicate left brain hemisphere (ipsilateral to MCAo) cytokines, blue asterisks indicate right brain hemisphere (contralateral to MCAo) cytokines. Control stroke male n = 3, Control stroke female n = 4, PAE stroke male n = 4, PAE stroke female n = 4.

and TNF-α were pro-inflammatory, and suppressed chemokines like G-CSF, GM-CSF, and Eotaxin are chemotactic agents that mobilize peripheral immune cells for diapedesis into target tissues. Consequently, PAE appears to have an overall inhibitory effect on the mechanisms for clearance of tissue damage in the acute phase of brain injury.

However, PAE results in more than brain-based disability, and FASD is a whole-body disorder.[11] For instance, PAE contributes to a hypertensive phenotype in young adult rodents[13,14] and adolescent humans[15] while also contributing to impaired glucose regulation[17,18] and renal dysfunction,[13] creating a physiological environment that results in worse recovery following cerebrovascular ischemic stroke.[19] Previous work showing links between cytokines of the mesenteric adipose and liver and physiological and behavioral outcomes[17] led us to ask whether transcriptomic differences in mesenteric adipose and liver as a result of PAE may explain some of the underlying etiology for the observed increase in negative outcomes post-stroke. In this study, we report that the mesenteric adipose and liver of healthy, stroke-naive 5 month-old young adult rats have minimal differences in gene expression due to prenatal experience. A more nuanced analysis of the transcriptome of these tissues identified TCA cycle as upregulated and rRNA processing as downregulated in the mesenteric adipose while dysregulation of necroptosis was identified in the liver. However, following stroke, we observed a far more exaggerated transcriptomic response in both the mesenteric adipose and liver of PAE animals. Moreover, the transcriptomic response to stroke in PAE offspring was substantially different from their age-matched, non-exposed controls. In the mesenteric adipose, there was significant upregulation of energy generating pathways that was unique to control animals while there was significant upregulation of cell cycle regulation pathways that was unique to PAE animals. In the liver, there was significant downregulation of triglyceride metabolism and upregulation of cholesterol/steroid metabolism that was unique to PAE animals while no pathways were identified using DEGs unique to control, suggesting instead perturbation of pathways that yet remain unidentified. Correlation of mesenteric adipose gene networks to recovery post-stroke identified gene networks with B/memory T cell differentiation, NF-κB signaling, mitochondrial transcription, and fatty acid biosynthetic process as relating to worse neural score. Correlation of liver gene networks to recovery post-stroke identified gene networks associated with negative regulation of IL-13/5/4 production as relating to worse neural score. Finally, cytokines of the brain hemisphere ipsilateral to the stroke, i.e., the damaged hemisphere, were related to specific gene networks in the mesenteric adipose as well as the liver. In the mesenteric adipose, the same cluster of cytokines were linked to modules that were unique to either PAE animals or control animals. In the liver, an expanded cluster of cytokines related to the same modules in PAE and control animals, yet these modules showed higher enrichment for PAE-unique DEGs, suggesting that PAE resulted in a larger hepatic response to stroke.

Table 1. Module enrichment for control and PAE-unique DEGs in mesenteric adipose that are correlated with stroked-hemisphere cytokines

Module	Control-Unique DEG enrichment	PAE-Unique DEG enrichment
darkgreen	0.038 (9/235)	0.064 (15/235)
midnightblue	0.016 (10/628)	0.016 (10/628)
magenta	0.059 (64/1088)	0.013 (14/1088)
pink	0.152 (166/1090)	0.049 (54/1090)

Parentheses indicate the ratio of DEGs to module genes.

In both the mesenteric adipose and liver of young adult stroke-naive rats, alterations in gene expression due to PAE were minimal when using strict FDR correction, suggesting, in the absence of adult-onset disease, shared cellular processes essential for survival and homeostasis were predominant drivers of transcriptome state. This is likely due to the fact that these animals were raised under the same conditions, in highly regulated husbandry environments with optimal nutrition, with the only difference being PAE, 5 months prior *in utero*. To gain a better understanding of more potentially more subtle baseline differences, we expanded our gene list of interest to include gene candidates (DRGs) that met three separate and independent statistical criteria ((1) unadjusted p value<0.05, (2) large effect size (Hedge's g > 0.8), and (3) nonoverlapping 95% confidence intervals around the mean of each treatment group), using a strategy identical to an approach we have previously used in our biomarker studies on FASD in human populations.[24]

In the mesenteric adipose tissue of stroke-naive rats, we identified a downregulation of rRNA processing genes as well as an upregulation of TCA cycle-associated genes. Ribosome biogenesis has previously been shown to be ethanol sensitive, with PAE decreasing ribosome-associated transcript expression during fetal development,[25,26] so this tendency for downregulation may persist in specific tissues such as the mesenteric adipose tissues throughout the lifespan. Ribosome synthesis is sensitive to environmental nutrient availability and metabolic challenges,[27] suggesting activation of the TCA cycle might be a compensatory attempt by adipocytes to increase the available energy supply to trigger enhanced ribosome production. This persistent low-level activation of the TCA cycle may prove maladaptive in the long run as it has been documented that increased TCA cycle activity and subsequent increase in TCA metabolites in white adipose tissue contribute to metabolic dysfunction, perturbing insulin sensitivity and secretory function of adipose.[28] Moreover, there may be less capacity for further TCA cycle activation in PAE animals post-stroke as only in control animal was there increased gene expression for energy production pathways in response to stroke, suggesting an inability of PAE animals to meet the new metabolic demands. In addition, mesenteric adipose gene networks enriched for NF-κB signaling were associated with the worse post-stroke recovery observed in PAE animals. Lipopolysaccharide (LPS) activates NF-κB signaling, triggering lipolysis in mesenteric adipose and a subsequent pro-inflammatory state.[29] Others have linked inflammation of the mesenteric adipose with worse prognosis after ischemic stroke and demonstrated that removal of visceral adipose tissue prior to stroke was protective and anti-inflammatory.[30] This implies that the enhanced NF-κB signaling observed in PAE mesenteric adipose tissue likely contributes to a heightened inflammatory response that plays a role in the worse recovery we observed in PAE animals.[19]

In the liver of stroke-naive rats, we observed even less of an effect of PAE on transcriptome state than in mesenteric adipose. However, in terms of response to an adult-onset health crisis, such as stroke, the liver exhibited a greatly enhanced response (DEGs: 1447 PAE v. 761, ~1.9-fold increase), showing that exposure to life stressors uncovers latent developmental programming differences that were initiated *in utero* because of PAE. This is consistent with what others have found, showing that it is only PAE in combination with adolescent stress that resulted in an exaggerated immune response after arthritis induction in adulthood.[31] Pathway analysis of genes unique to PAE response to stroke identified upregulation of cholesterol biosynthesis, suggesting potential elevation of cholesterol levels. Normally, there is a decrease in cholesterol levels after ischemic events, such as myocardial infarction[32] and ischemic stroke.[33] Moreover, a meta-analysis found that initiation of statin use after stroke potentially decreases risk of post-stroke symptomatic intracranial hemorrhage,[34] suggesting elevated cholesterol levels may be detrimental, and consequently, the elevation in genes associated with cholesterol biosynthesis in PAE animals may contribute to the observed impaired recovery.[19] Furthermore, gene networks negatively regulating production of IL-4/5/13 were associated with the worse post-stroke recovery observed in PAE animals. These are anti-inflammatory cytokines typically associated with T_H2 cells, and lower levels in circulation were prognostic for more severe stroke in human patients.[35] Specifically, both IL-4[36] and IL-13[37,38] were shown to promote an anti-inflammatory phenotype in microglia (M2) and promote long-term stroke recovery. Thus, this weakened anti-inflammatory response in the liver may also contribute to worse stroke outcomes in PAE animals.

Correlational analysis revealed a link between cytokines of the stroke-damaged hemisphere and specific gene networks of the mesenteric adipose as well as the liver in young adult animals post-stroke. Though this linkage by itself does not imply a causal relationship, it is likely that in this instance brain inflammation after stroke is the immediate, proximate cause, and changes in gene expression in mesenteric adipose tissue and the liver are an adaptive consequence. This hypothesis is supported by data which document that the brain can communicate directly with the gut,[39] mesenteric adipose,[40,41] and liver[42,43] via the vagus nerve, and that this communication with the gut influences stroke outcomes.[39] The cluster of cytokines within the stroke-damaged hemisphere that were consistently associated with mesenteric adipose tissue

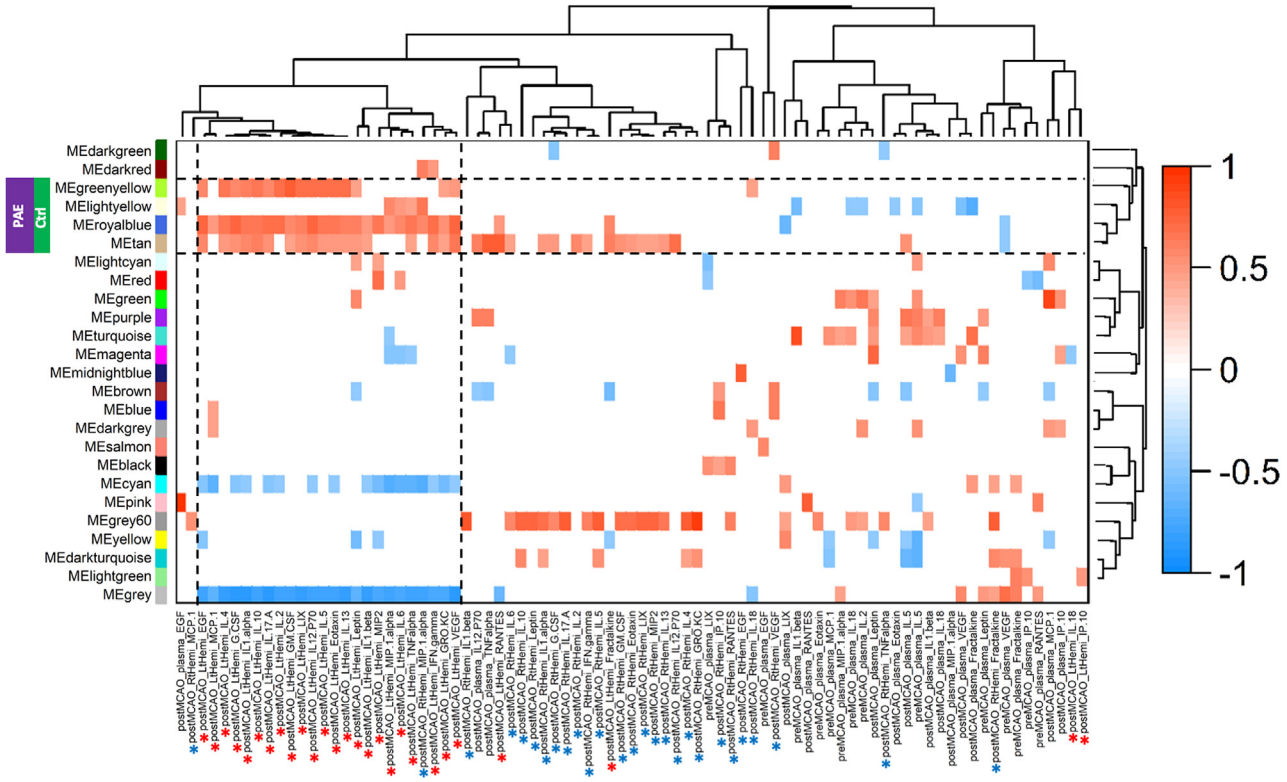

Figure 9. WGCNA reveals gene networks of the liver associated with ischemic hemisphere cytokines

Heatmap of module-trait relationships depicting correlations between module eigengenes (ME) and fetal-placenta growth parameters. Only significant ($p < 0.05$) and trending ($0.05 < p < 0.1$) correlations are shown. The degree of correlation (r) is illustrated with the color legend. Red asterisks indicate left brain hemisphere (ipsilateral to MCAo) cytokines, blue asterisks indicate right brain hemisphere (contralateral to MCAo) cytokines. Control stroke male n = 3, Control stroke female n = 4, PAE stroke male n = 4, PAE stroke female n = 4.

and liver gene networks, EGF, MCP1, IL-4, G-CSF, IL-1α, IL-17A, IL-2, GM-CSF, LIX, IL-12p70, IL-5, Eotaxin, and IL-13, constitute a mix of mostly pro- and some anti-inflammatory cytokines, suggesting that the correlated network of brain cytokines and peripheral tissue gene modules includes both exacerbating and mitigating components. Whether specific stimulated gene networks in enteric organs is compensatory or maladaptive remains to be determined. Additionally, the impact of PAE on these cytokine-associated gene modules was different in mesenteric adipose tissue compared to its portal efferent, the liver. In mesenteric adipose tissue, modules that correlated with cytokine levels post-stroke were differentially enriched for PAE-unique DEGs, with control-unique, post-stroke DEGs, sub-clustering separately. This suggests the PAE programs mesenteric adipose tissue to respond differently to the same adult-onset disease trigger compared to matched, non-prenatally exposed controls. In contrast, in the liver, modules that correlated with cytokine levels contained genes from PAE-unique and control-unique DEGs, but PAE-unique DEGS were ~2-fold higher in each module, suggesting similar pathway activation in response to the same signal but a more pronounced response in the liver of PAE animals. Whether these altered responses to cerebral cytokine levels in PAE is compensatory or contributes to worse recovery post-stroke is an avenue for future studies.

A key strength of this study was the direct test of the developmental origins of the adult health and disease hypothesis where we found that PAE, an early life adversity, modified the brain and systemic response to an acute adult-onset disease, stroke. In this context the use of a "within-subjects" design with the litter as the unit of analysis facilitated the assessment of associations between brain changes and enteric portal tissue outcomes. Collectively, our findings suggest that PAE inhibits the brain cytokine response to a severe adult-onset health crisis such as cerebrovascular ischemic stroke and, moreover, reprograms the mesenteric adipose and liver to behave maladaptively in response to that stroke. However, since stroke-naive healthy young adult rats had minimal transcriptomic differences in the mesenteric adipose and liver, these maladaptations are normally latent and, as our data indicate, only uncovered in response to a health stressor. Moreover, since animal housing and other husbandry conditions were identical between PAE and non-exposed control offspring, our data also suggest that common cellular processes for survival and homeostasis are predominant drivers of transcriptome state, minimizing all but the more subtle and nuanced differences in stroke-naive animals. Finally, both male and female offspring were used in this study, and though there were sex differences, we were also able to identify sex-independent effects of PAE on stroke outcomes.

These data support a strategy for proactive prevention of disease in individuals with FASD that may be crucial for preventing adverse health outcomes that contribute to the higher mortality rate observed in this population. Our work suggests that PAE programs for activation of unique pathways in response to a health crisis that are more pro-inflammatory and maladaptive in comparison to their control counterparts.

Table 2. Module enrichment for control and PAE-unique DEGs in liver that are correlated with stroked-hemisphere cytokines

Module	Control-Unique DEG enrichment	PAE-Unique DEG enrichment
greenyellow	0.002 (8/720)	0.014 (10/720)
lightyellow	0.002 (5/468)	0.038 (18/476)
royalblue	0.011 (5/468)	0.036 (17/468)
tan	0.006 (4/709)	0.048 (34/709)

Parentheses indicate the ratio of DEGs to module genes.

Future studies in a new cohort of animals will be required to validate these findings. Moreover, continued work is needed to identify points of prevention and intervention, and personalized medicine may be needed for individuals with FASD due to PAE-unique responses to disease.

Limitations of the study

An important limitation of this study relates to experimental design considerations in that we elected to not perform a sham surgery (including anesthesia and needle insertion into the brain) on our stroke-naive animals. We chose this strategy because needle insertion recapitulates the "stab injury" model of traumatic brain injury[44] and is by itself an acute adult-onset disease model. Therefore, in this study, the stroke exposure experience included the effects of both needle insertion and endothelin-1. However, we document here, in a different cohort of animals, that a sham surgery did not result in elevated circulating inflammatory cytokines suggesting no effect on systemic inflammation.

STAR★METHODS

Detailed methods are provided in the online version of this paper and include the following:

- KEY RESOURCES TABLE
- RESOURCE AVAILABILITY
  - Lead contact
  - Materials availability
  - Data and code availability
- EXPERIMENTAL MODEL AND SUBJECT DETAILS
- METHOD DETAILS
  - Rat model of PAE
  - Middle cerebral artery occlusion (MCAo)
  - Neurological score
  - Extraction of tissues and blood Isolation
  - Cytokine assays
  - RNA Isolation and RNA Library preparation and sequencing
- QUANTIFICATION AND STATISTICAL ANALYSIS

SUPPLEMENTAL INFORMATION

Supplemental information can be found online at https://doi.org/10.1016/j.isci.2023.107920.

ACKNOWLEDGMENTS

Portions of this research were conducted with high-performance research computing resources provided by Texas A&M University (https://hprc.tamu.edu). This work was supported by grants from the NIH, R01 AA026756 (FS, RCM) and F30 AA027698 (MRP).

AUTHOR CONTRIBUTIONS

Conceptualization: MRP, FS, and RCM; Methodology: MRP, SB, FS, and RCM; Investigation: MRP, SB, DAH, and NTS; Validation, SB, DAH, and NTS; Formal Analysis, MRP, FS, and RCM; Visualization: MRP, DAH, NTS, and RCM; Data Curation: MRP, FS, and RCM; Writing – Original Draft: MRP, SB, DAH, and NTS; Writing – Review & Editing: MRP, SB, FS, and RCM; Funding Acquisition: MRP, FS, and RCM; Supervision: FS and RCM.

DECLARATION OF INTERESTS

The authors declare no competing interests.

INCLUSION AND DIVERSITY

We worked to ensure sex balance in the selection of non-human subjects. We support inclusive, diverse, and equitable conduct of research.

Received: November 19, 2022
Revised: July 24, 2023
Accepted: September 12, 2023
Published: September 13, 2023

REFERENCES

1. Barker, D.J., Gluckman, P.D., Godfrey, K.M., Harding, J.E., Owens, J.A., and Robinson, J.S. (1993). Fetal nutrition and cardiovascular disease in adult life. Lancet *341*, 938–941. https://doi.org/10.1016/0140-6736(93)91224-A.
2. Weeks, O., Bossé, G.D., Oderberg, I.M., Akle, S., Houvras, Y., Wrighton, P.J., LaBella, K., Iversen, I., Tavakoli, S., Adatto, I., et al. (2020). Fetal alcohol spectrum disorder predisposes to metabolic abnormalities in adulthood. J. Clin. Invest. *130*, 2252–2269. https://doi.org/10.1172/JCI132139.
3. Lunde, E.R., Washburn, S.E., Golding, M.C., Bake, S., Miranda, R.C., and Ramadoss, J. (2016). Alcohol-Induced Developmental Origins of Adult-Onset Diseases. Alcohol Clin. Exp. Res. *40*, 1403–1414. https://doi.org/10.1111/acer.13114.
4. Bakhireva, L.N., Sharkis, J., Shrestha, S., Miranda-Sohrabji, T.J., Williams, S., and Miranda, R.C. (2017). Prevalence of Prenatal Alcohol Exposure in the State of Texas as Assessed by Phosphatidylethanol in Newborn Dried Blood Spot Specimens. Alcohol Clin. Exp. Res. *41*, 1004–1011. https://doi.org/10.1111/acer.13375.
5. Umer, A., Lilly, C., Hamilton, C., Baldwin, A., Breyel, J., Tolliver, A., Mullins, C., John, C., and Maxwell, S. (2020). Prevalence of alcohol use in late pregnancy. Pediatr. Res. *88*, 312–319. https://doi.org/10.1038/s41390-019-0731-y.
6. DiBattista, A., Ogrel, S., MacKenzie, A.E., and Chakraborty, P. (2022). Quantitation of phosphatidylethanols in dried blood spots to determine rates of prenatal alcohol exposure in Ontario. Alcohol Clin. Exp. Res. *46*, 243–251. https://doi.org/10.1111/acer.14766.
7. May, P.A., Chambers, C.D., Kalberg, W.O., Zellner, J., Feldman, H., Buckley, D., Kopald, D., Hasken, J.M., Xu, R., Honerkamp-Smith, G., et al. (2018). Prevalence of fetal alcohol spectrum disorders in 4 us communities. JAMA *319*, 474–482. https://doi.org/10.1001/jama.2017.21896.
8. May, P.A., and Gossage, J.P. (2001). Estimating the prevalence of fetal alcohol syndrome. A summary. Alcohol Res. Health *25*, 159–167.
9. Riley, E.P., Infante, M.A., and Warren, K.R. (2011). Fetal alcohol spectrum disorders: an overview. Neuropsychol. Rev. *21*, 73–80. https://doi.org/10.1007/s11065-011-9166-x.
10. Moore, E.M., and Riley, E.P. (2015). What Happens When Children with Fetal Alcohol Spectrum Disorders Become Adults? Curr. Dev. Disord. Rep. *2*, 219–227. https://doi.org/10.1007/s40474-015-0053-7.
11. Himmelreich, M., Lutke, C.J., and Hargrove, E.T. (2020). The lay of the land: Fetal alcohol spectrum disorder (FASD) as a whole-body diagnosis. In The Routledge Handbook of Social Work and Addictive Behaviors, A.L. Begun and M.M. Murray, eds. (Routledge).
12. Thanh, N.X., and Jonsson, E. (2016). Life Expectancy of People with Fetal Alcohol Syndrome. J. Popul. Therapeut. Clin. Pharmacol. *23*, e53–e59.
13. Gray, S.P., Denton, K.M., Cullen-McEwen, L., Bertram, J.F., and Moritz, K.M. (2010). Prenatal exposure to alcohol reduces nephron number and raises blood pressure in progeny. J. Am. Soc. Nephrol. *21*, 1891–1902. https://doi.org/10.1681/ASN.2010040368.
14. Bake, S., Gardner, R., Tingling, J.D., Miranda, R.C., and Sohrabji, F. (2017). Fetal Alcohol Exposure Alters Blood Flow and Neurological Responses to Transient Cerebral Ischemia in Adult Mice. Alcohol Clin. Exp. Res. *41*, 117–127. https://doi.org/10.1111/acer.13277.
15. Cook, J.C., Lynch, M.E., and Coles, C.D. (2019). Association Analysis: Fetal Alcohol Spectrum Disorder and Hypertension Status in Children and Adolescents. Alcohol Clin. Exp. Res. *43*, 1727–1733. https://doi.org/10.1111/acer.14121.
16. Cipolla, M.J., Liebeskind, D.S., and Chan, S.L. (2018). The importance of comorbidities in ischemic stroke: Impact of hypertension on the cerebral circulation. J. Cerebr. Blood Flow Metabol. *38*, 2129–2149. https://doi.org/10.1177/0271678X18800589.
17. Bake, S., Pinson, M.R., Pandey, S., Chambers, J.P., Mota, R., Fairchild, A.E., Miranda, R.C., and Sohrabji, F. (2021). Prenatal alcohol-induced sex differences in immune, metabolic and neurobehavioral outcomes in adult rats. Brain Behav. Immun. *98*, 86–100. https://doi.org/10.1016/j.bbi.2021.08.207.
18. Nguyen, T.M.T., Steane, S.E., Moritz, K.M., and Akison, L.K. (2019). Prenatal alcohol exposure programmes offspring disease: insulin resistance in adult males in a rat model of acute exposure. J. Physiol. *597*, 5619–5637. https://doi.org/10.1113/JP278531.
19. Bake, S., Hurst, D.A., Miranda, R.C., and Sohrabji, F. (2022). Prenatal alcohol exposure exacerbates acute sensorimotor deficits and impedes long-term behavioral recovery from the effects of an adult-onset cerebrovascular ischemic stroke. Alcohol Clin. Exp. Res. *46*, 2267–2279. https://doi.org/10.1111/acer.14952.
20. Arya, A.K., and Hu, B. (2018). Brain-gut axis after stroke. Brain Circ. *4*, 165–173. https://doi.org/10.4103/bc.bc_32_18.
21. El-Hakim, Y., Mani, K.K., Eldouh, A., Pandey, S., Grimaldo, M.T., Dabney, A., Pilla, R., and Sohrabji, F. (2021). Sex differences in stroke outcome correspond to rapid and severe changes in gut permeability in adult Sprague-Dawley rats. Biol. Sex Differ. *12*, 14. https://doi.org/10.1186/s13293-020-00352-1.
22. Mani, K.K., El-Hakim, Y., Branyan, T.E., Samiya, N., Pandey, S., Grimaldo, M.T., Habbal, A., Wertz, A., and Sohrabji, F. (2023). Intestinal Epithelial Stem Cell Transplants as a Novel Therapy for Cerebrovascular Stroke. Brain Behav. Immun. *107*, 345–360. https://doi.org/10.1016/j.bbi.2022.10.015.
23. Konrad, D., and Wueest, S. (2014). The Gut-Adipose-Liver Axis in the Metabolic Syndrome. Physiology *29*, 304–313. https://doi.org/10.1152/physiol.00014.2014.
24. Mahnke, A.H., Sideridis, G.D., Salem, N.A., Tseng, A.M., Carter, R.C., Dodge, N.C., Rathod, A.B., Molteno, C.D., Meintjes, E.M., Jacobson, S.W., et al. (2021). Infant circulating MicroRNAs as biomarkers of effect in fetal alcohol spectrum disorders. Sci. Rep. *11*, 1429. https://doi.org/10.1038/s41598-020-80734-y.
25. Berres, M.E., Garic, A., Flentke, G.R., and Smith, S.M. (2017). Transcriptome Profiling Identifies Ribosome Biogenesis as a Target of Alcohol Teratogenicity and Vulnerability during Early Embryogenesis. PLoS One *12*, e0169351. https://doi.org/10.1371/journal.pone.0169351.
26. Salem, N.A., Mahnke, A.H., Konganti, K., Hillhouse, A.E., and Miranda, R.C. (2021). Cell-type and fetal-sex-specific targets of prenatal alcohol exposure in developing mouse cerebral cortex. iScience *24*, 102439. https://doi.org/10.1016/j.isci.2021.102439.
27. Liu, L., and Pilch, P.F. (2016). PTRF/Cavin-1 promotes efficient ribosomal RNA transcription in response to metabolic challenges. Elife *5*, e17508. https://doi.org/10.7554/eLife.17508.
28. Nagao, H., Nishizawa, H., Bamba, T., Nakayama, Y., Isozumi, N., Nagamori, S., Kanai, Y., Tanaka, Y., Kita, S., Fukuda, S., et al. (2017). Increased Dynamics of Tricarboxylic Acid Cycle and Glutamate Synthesis in Obese Adipose Tissue: In Vivo Metabolic Turnover Analysis. J. Biol. Chem. *292*, 4469–4483. https://doi.org/10.1074/jbc.M116.770172.
29. Grisouard, J., Bouillet, E., Timper, K., Radimerski, T., Dembinski, K., Frey, D.M., Peterli, R., Zulewski, H., Keller, U., Müller, B., and Christ-Crain, M. (2012). Both inflammatory and classical lipolytic pathways are involved in lipopolysaccharide-induced lipolysis in human adipocytes. Innate Immun. *18*, 25–34. https://doi.org/10.1177/1753425910386632.

30. Shin, J.A., Jeong, S.I., Kim, M., Yoon, J.C., Kim, H.-S., and Park, E.-M. (2015). Visceral adipose tissue inflammation is associated with age-related brain changes and ischemic brain damage in aged mice. Brain Behav. Immun. *50*, 221–231. https://doi.org/10.1016/j.bbi.2015.07.008.
31. Bodnar, T.S., Mak, D.Y., Hill, L.A., Ellis, L., Yu, W., and Weinberg, J. (2022). Modulatory role of prenatal alcohol exposure and adolescent stress on the response to arthritis challenge in adult female rats. EBioMedicine *77*, 103876. https://doi.org/10.1016/j.ebiom.2022.103876.
32. Wattanasuwan, N., Khan, I.A., Gowda, R.M., Vasavada, B.C., and Sacchi, T.J. (2001). Effect of Acute Myocardial Infarction on Cholesterol Ratios. Chest *120*, 1196–1199. https://doi.org/10.1378/chest.120.4.1196.
33. Yan, B., Parsons, M., McKay, S., Campbell, D., Infeld, B., Czajko, R., and Davis, S.M. (2005). When to Measure Lipid Profile after Stroke? Cerebrovasc. Dis. *19*, 234–238. https://doi.org/10.1159/000084086.
34. Tan, C., Liu, X., Mo, L., Wei, X., Peng, W., Wang, H., Zhou, W., Jiang, J., Chen, Y., and Chen, L. (2019). Statin, cholesterol, and sICH after acute ischemic stroke: systematic review and meta-analysis. Neurol. Sci. *40*, 2267–2275. https://doi.org/10.1007/s10072-019-03995-0.
35. Li, X., Lin, S., Chen, X., Huang, W., Li, Q., Zhang, H., Chen, X., Yang, S., Jin, K., and Shao, B. (2019). The Prognostic Value of Serum Cytokines in Patients with Acute Ischemic Stroke. Aging Dis. *10*, 544–556. https://doi.org/10.14336/AD.2018.0820.
36. Liu, X., Liu, J., Zhao, S., Zhang, H., Cai, W., Cai, M., Ji, X., Leak, R.K., Gao, Y., Chen, J., and Hu, X. (2016). Interleukin-4 Is Essential for Microglia/Macrophage M2 Polarization and Long-Term Recovery After Cerebral Ischemia. Stroke *47*, 498–504. https://doi.org/10.1161/STROKEAHA.115.012079.
37. Kolosowska, N., Keuters, M.H., Wojciechowski, S., Keksa-Goldsteine, V., Laine, M., Malm, T., Goldsteins, G., Koistinaho, J., and Dhungana, H. (2019). Peripheral Administration of IL-13 Induces Anti-inflammatory Microglial/Macrophage Responses and Provides Neuroprotection in Ischemic Stroke. Neurotherapeutics *16*, 1304–1319. https://doi.org/10.1007/s13311-019-00761-0.
38. Hamzei Taj, S., Le Blon, D., Hoornaert, C., Daans, J., Quarta, A., Praet, J., Van der Linden, A., Ponsaerts, P., and Hoehn, M. (2018). Targeted intracerebral delivery of the anti-inflammatory cytokine IL13 promotes alternative activation of both microglia and macrophages after stroke. J. Neuroinflammation *15*, 174. https://doi.org/10.1186/s12974-018-1212-7.
39. Durgan, D.J., Lee, J., McCullough, L.D., and Bryan, R.M. (2019). Examining the Role of the Microbiota-Gut-Brain Axis in Stroke. Stroke *50*, 2270–2277. https://doi.org/10.1161/STROKEAHA.119.025140.
40. Nguyen, N.L.T., Randall, J., Banfield, B.W., and Bartness, T.J. (2014). Central sympathetic innervations to visceral and subcutaneous white adipose tissue. Am. J. Physiol. Regul. Integr. Comp. Physiol. *306*, R375–R386. https://doi.org/10.1152/ajpregu.00552.2013.
41. Kreier, F., Fliers, E., Voshol, P.J., Van Eden, C.G., Havekes, L.M., Kalsbeek, A., Van Heijningen, C.L., Sluiter, A.A., Mettenleiter, T.C., Romijn, J.A., et al. (2002). Selective parasympathetic innervation of subcutaneous and intra-abdominal fat–functional implications. J. Clin. Invest. *110*, 1243–1250. https://doi.org/10.1172/JCI15736.
42. Wong, C.H.Y., Jenne, C.N., Lee, W.-Y., Léger, C., and Kubes, P. (2011). Functional Innervation of Hepatic iNKT Cells Is Immunosuppressive Following Stroke. Science *334*, 101–105. https://doi.org/10.1126/science.1210301.
43. Mizuno, K., and Ueno, Y. (2017). Autonomic Nervous System and the Liver. Hepatol. Res. *47*, 160–165. https://doi.org/10.1111/hepr.12760.
44. Fan, Q., Takarada-Iemata, M., Okitani, N., Tamatani, T., Ishii, H., Hattori, T., Kiryu-Seo, S., Kiyama, H., and Hori, O. (2023). Brain injury triggers cell-type-specific and time-dependent endoplasmic reticulum stress responses. Glia *71*, 667–681. https://doi.org/10.1002/glia.24303.
45. Bolger, A.M., Lohse, M., and Usadel, B. (2014). Trimmomatic: a flexible trimmer for Illumina sequence data. Bioinformatics *30*, 2114–2120. https://doi.org/10.1093/bioinformatics/btu170.
46. Kim, D., Langmead, B., and Salzberg, S.L. (2015). HISAT: a fast spliced aligner with low memory requirements. Nat. Methods *12*, 357–360. https://doi.org/10.1038/nmeth.3317.
47. Anders, S., Pyl, P.T., and Huber, W. (2015). HTSeq–a Python framework to work with high-throughput sequencing data. Bioinformatics *31*, 166–169. https://doi.org/10.1093/bioinformatics/btu638.
48. Love, M.I., Huber, W., and Anders, S. (2014). Moderated estimation of fold change and dispersion for RNA-seq data with DESeq2. Genome Biol. *15*, 550. https://doi.org/10.1186/s13059-014-0550-8.
49. Blighe, K., Rana, S., and Lewis, M. (2021). EnhancedVolcano: Publication-Ready Volcano Plots with Enhanced Colouring and Labeling (Bioconductor).
50. Yu, G., and He, Q.-Y. (2016). ReactomePA: an R/Bioconductor package for reactome pathway analysis and visualization. Mol. Biosyst. *12*, 477–479. https://doi.org/10.1039/C5MB00663E.
51. Kanehisa, M., Furumichi, M., Tanabe, M., Sato, Y., and Morishima, K. (2017). KEGG: new perspectives on genomes, pathways, diseases and drugs. Nucleic Acids Res. *45*, D353–D361. https://doi.org/10.1093/nar/gkw1092.
52. Luo, W., and Brouwer, C. (2013). Pathview: an R/Bioconductor package for pathway-based data integration and visualization. Bioinformatics *29*, 1830–1831. https://doi.org/10.1093/bioinformatics/btt285.
53. Mouton, A.J., Maxi, J.K., Souza-Smith, F., Bagby, G.J., Gilpin, N.W., Molina, P.E., and Gardner, J.D. (2016). Alcohol Vapor Inhalation as a Model of Alcohol-Induced Organ Disease. Alcohol Clin. Exp. Res. *40*, 1671–1678. https://doi.org/10.1111/acer.13133.
54. Crabbe, J.C., Harris, R.A., and Koob, G.F. (2011). Preclinical studies of alcohol binge drinking. Ann. N. Y. Acad. Sci. *1216*, 24–40. https://doi.org/10.1111/j.1749-6632.2010.05895.x.
55. Adachi, J., Mizoi, Y., Fukunaga, T., Ogawa, Y., Ueno, Y., and Imamichi, H. (1991). Degrees of alcohol intoxication in 117 hospitalized cases. J. Stud. Alcohol *52*, 448–453.
56. Selvamani, A., and Sohrabji, F. (2010). The neurotoxic effects of estrogen on ischemic stroke in older female rats is associated with age-dependent loss of insulin-like growth factor-1. J. Neurosci. *30*, 6852–6861. https://doi.org/10.1523/JNEUROSCI.0761-10.2010.
57. Selvamani, A., Sathyan, P., Miranda, R.C., and Sohrabji, F. (2012). An Antagomir to MicroRNA Let7f Promotes Neuroprotection in an Ischemic Stroke Model. PLoS One *7*, e32662. https://doi.org/10.1371/journal.pone.0032662.
58. Balden, R., Selvamani, A., and Sohrabji, F. (2012). Vitamin D Deficiency Exacerbates Experimental Stroke Injury and Dysregulates Ischemia-Induced Inflammation in Adult Rats. Endocrinology *153*, 2420–2435. https://doi.org/10.1210/en.2011-1783.
59. Selvamani, A., Williams, M.H., Miranda, R.C., and Sohrabji, F. (2014). Circulating miRNA profiles provide a biomarker for severity of stroke outcomes associated with age and sex in a rat model. Clin. Sci. *127*, 77–89. https://doi.org/10.1042/cs20130565.
60. Selvamani, A., and Sohrabji, F. (2017). Mir363-3p improves ischemic stroke outcomes in female but not male rats. Neurochem. Int. *107*, 168–181. https://doi.org/10.1016/j.neuint.2016.10.008.
61. Panta, A., Pandey, S., Duncan, I.N., Duhamel, S., and Sohrabji, F. (2019). Mir363-3p attenuates post-stroke depressive-like behaviors in middle-aged female rats. Brain Behav. Immun. *78*, 31–40. https://doi.org/10.1016/j.bbi.2019.01.003.
62. Albers, G.W., Goldstein, L.B., Hess, D.C., Wechsler, L.R., Furie, K.L., Gorelick, P.B., Hurn, P., Liebeskind, D.S., Nogueira, R.G., and Saver, J.L.; STAIR VII Consortium (2011). Stroke Treatment Academic Industry Roundtable (STAIR) Recommendations for Maximizing the Use of Intravenous Thrombolytics and Expanding Treatment Options With Intra-arterial and Neuroprotective Therapies. Stroke *42*, 2645–2650. https://doi.org/10.1161/STROKEAHA.111.618850.
63. Langfelder, P., and Horvath, S. (2008). WGCNA: an R package for weighted correlation network analysis. BMC Bioinf. *9*, 559. https://doi.org/10.1186/1471-2105-9-559.

STAR★METHODS

KEY RESOURCES TABLE

REAGENT or RESOURCE	SOURCE	IDENTIFIER
Chemicals, peptides, and recombinant proteins		
Ethanol, ACS grade	Acros Orgnics	#61511
Endothelin-1	American Peptide Company INC	#4040254
RIPA buffer	Sigma-Aldrich, MO	#R0278
Critical commercial assays		
Thermo Scientific Pierce BCA Protein Assay kit	Fisher Scientific, MA	#P123227
MILLIPLEX MAP Rat Cytokine Multiplexed bead assay	Millipore Corp, MA	#RECYMAG65K27PMX
miRNeasy mini kit	Qiagen, MD	#217004
TruSeq Stranded Total RNA	Illumina; San Diego, CA	#20040529
QScript cDNA synthesis kit	Quanta Bio/Avantor, UK	VWR #101414
PerfeCTa SYBR Green FastMix, ROX Reaction Mix	Quanta Bio, MA	#95073-012
Deposited data		
GSE217173	NCBI GEO (https://www.ncbi.nlm.nih.gov/geo/query/acc.cgi)	Gene Expression Omnibus (GEO) (RRID:SCR_005012)
Experimental models: Organisms/strains		
Sprague-Dawley Rats	Envigo/Inotiv, TX	Hsd:Sprague Dawley® SD® #002; RRID:RGD_737903
Oligonucleotides		
Slc25a25, Forward Primer, 5′-AACCCGGCATTCCCTACTCT-3′	Life Technologies, TX	Custom Order #10336022
Slc25a25, Reverse Primer, 5′-AGTCCAGTTGCCCATCAAGG-3′	Life Technologies, TX	Custom Order #10336022
C5, Forward Primer, 5′-CATCAGGGCCTTCAACGAGT-3′	Life Technologies, TX	Custom Order #10336022
C5, Reverse Primer, 5′-TTGGATCTGCTCCCCTCGTA-3′	Life Technologies, TX	Custom Order #10336022
Fads2, Forward Primer, 5′-TAGAAGACAAAAGCTGAAAGCGA-3′	Life Technologies, TX	Custom Order #10336022
Fads2, Reverse Primer, 5′-GAACTTGCCCACGAAATCCAG-3′	Life Technologies, TX	Custom Order #10336022
Fads2, Reverse Primer, 5′-GAACTTGCCCACGAAATCCAG-3′	Life Technologies, TX	Custom Order #10336022
Calr, Reverse Primer, 5′-TGGCCTCTACAGCTCATCCT-3′	Life Technologies, TX	Custom Order #10336022
Tat, Forward Primer, 5′-TCAGTAAGCGGCACCTTCAG-3′	Life Technologies, TX	Custom Order #10336022
Tat, Reverse Primer, 5′-AGAGGTCCGCATTGGACTTG-3′	Life Technologies, TX	Custom Order #10336022
Agxt, Forward Primer, 5′-TAGCTGGGAAATGTTCCGGATG-3′	Life Technologies, TX	Custom Order #10336022
Agxt, Reverse Primer, 5′-CCACCTCCTGCAGTGTGTAAT-3′	Life Technologies, TX	Custom Order #10336022

(*Continued on next page*)

Continued

REAGENT or RESOURCE	SOURCE	IDENTIFIER
Thrsp, Forward Primer, 5′-GACCTAGAAGCCCAGTTCCAC-3′	Life Technologies, TX	Custom Order #10336022
Thrsp, Reverse Primer, 5′-CGCTTGCTATTACCTCTGCCT-3′	Life Technologies, TX	Custom Order #10336022
FADS1, Forward Primer, 5′-CCACTACGCTGGTCAGGATG-3′	Life Technologies, TX	Custom Order #10336022
FADS1, Reverse Primer, 5′-AGCGCCTTATTCTTGGTGGG-3′	Life Technologies, TX	Custom Order #10336022
HP, Forward Primer, 5′-ATCGCTGCCGACAGTTCTAC-3′	Life Technologies, TX	Custom Order #10336022
HP, Reverse Primer, 5′-GGCGCTACGTAGTCTTTGGA-3′	Life Technologies, TX	Custom Order #10336022
Acly, Forward Primer, 5′-TACGGACAGAGAGCCACACT-3′	Life Technologies, TX	Custom Order #10336022
Acly, Reverse Primer, 5′-ACCAAGCTTTCCTCGACGTT-3′	Life Technologies, TX	Custom Order #10336022
Insig1, Forward Primer, 5′-GTCTGGAGCTACCCAAGCG-3′	Life Technologies, TX	Custom Order #10336022
Insig1, Reverse Primer, 5′-TGGCGAAATCTAATTTGGCACTG-3′	Life Technologies, TX	Custom Order #10336022
Slc38a2, Forward Primer, 5′-TGTGGGCAGTGGAATCCTTG-3′	Life Technologies, TX	Custom Order #10336022
Slc38a2, Reverse Primer, 5′-GAGCACGAAGGACACCAGAA-3′	Life Technologies, TX	Custom Order #10336022
Fasn, Forward Primer, 5′-GTGGAAGACACTGGCTCGAA-3′	Life Technologies, TX	Custom Order #10336022
Fasn, Reverse Primer, 5′-TGGTACACTTTCCCGCTCAC-3′	Life Technologies, TX	Custom Order #10336022
Itih4, Forward Primer, 5′-GACATTGTCCAGACTCGGGG-3′	Life Technologies, TX	Custom Order #10336022
Itih4, Reverse Primer, 5′-GGCAGGATGATGGTAGGAGC-3′	Life Technologies, TX	Custom Order #10336022
Software and algorithms		
GraphPad Prism, version 9.2.0	GraphPad Software, MA	GraphPad Prism (RRID:SCR_002798)
Stata Base Edition, version 18.0	STATA Corp LLC, TX	Stata (RRID:SCR_012763)
Trimmomatic	Bolger et al.,[45]	Trimmomatic (RRID:SCR_011848)
Hisat2 version 2.1.0	Kim et al.,[46]	HISAT2 (RRID:SCR_015530)
HTSeq	Anders et al.,[47]	HTSeq (RRID:SCR_005514)
DESeq2 version 2.1.8.3	Love et al.,[48]	DESeq2 (RRID:SCR_015687)
Galaxy	https://galaxyproject.org/	Galaxy (RRID:SCR_006281)
EnhancedVolcano	Blighe et al.,[49]	EnhancedVolcano (RRID:SCR_018931)
ReactomePA	Yu and He,[50]	ReactomePA (RRID:SCR_019316)
Pathview R	Kaneshia et al.,[51]	Pathview (RRID:SCR_002732)
WGCNA R	Luo and Brouwer[52]	Weighted Gene Co-expression Network Analysis (RRID:SCR_003302)

RESOURCE AVAILABILITY

Lead contact

Requests for further information and for resources and reagents should be directed to and will be fulfilled by the lead contact, Dr. Rajesh C. Miranda (rmiranda@tamu.edu).

Materials availability

This study generated new primer sequences for analyzing mRNA transcripts by qRT-PCR. Forward and reverse primer sequences are detailed in the key resources table.

Data and code availability

- RNAseq expression data generated during this study are available in the NCBI/GEO database (accession number, GSE217173).
- All data reported in this paper will be shared by the lead contact upon request.
- This paper does not report original code.

Any additional information required to reanalyze the data reported in this paper is available from the lead contact upon request.

EXPERIMENTAL MODEL AND SUBJECT DETAILS

This study utilized adult male and female Sprague Dawley rats, purchased from Envigo Laboratories, TX, and pair-housed in same-sex groups at the Texas A&M University vivarium, until breeding to generate pregnant females. As previously published, Sprague-Dawley dams and males were caged together overnight for a timed-mating, and gestational day 0 (GD0) was defined as the start of the mating period.[17] Following mating, pregnant dams were randomly assigned to control or prenatal alcohol exposure (PAE) groups. Litters were culled to n = 10/ litter by postnatal day 3 and pups were weaned at postnatal day 21 and pair-housed with littermates of the same sex in a standard rat cage. Offspring of both sexes were used for subsequent studies. All procedures were conducted under a protocol approved by the Texas A&M University Institutional Animal Care and Use Committee (protocol #2020-0265).

METHOD DETAILS

Rat model of PAE

Our exposure paradigm was the same as we have previously published[17] and tissue from the same animals were used in the present study. Briefly, Sprague-Dawley dams (2 females/cage) were exposed to alcohol vapor (95%, ACS grade, Acros Organics, NJ # 61511) at a flow rate of 10 mL/min for 1 h daily for 12 days starting at gestational day (GD) 8 between 9:00-10:00 am. This whole-body exposure model of chronic-intermittent exposure is commonly used in rodent models of alcohol dependence (reviewed in[53,54]) and results in accurate attainment of target maternal blood ethanol concentrations (BECs) at levels attained in human populations, in persons with alcohol use disorders.[55] Control animals were handled the same way and received ambient air for the same duration as the alcohol vapor. Animals were monitored for signs of distress before being returned to home cages every day. Average BEC was 299 $\pm$ 52 mg/dL (across the entire treatment period).

Middle cerebral artery occlusion (MCAo)

The main aim of this study was to compare the effects of a single adverse life event, PAE, to the modifying effects of PAE on the response to adult-onset disease. Therefore, at 5 months, stroke was induced in both male and female offspring by intracerebral injection of vasoconstrictive peptide Endothelin-1 (ET-1, American Peptide Company INC; 0.5ug/ul, 600 pmol; 3 uls) using stereotaxic co-ordinates (AP: +0.9, ML: −3.4, DV: −8.5) as described in our previous work.[56–61] Body temperature was maintained at 37°C throughout the surgery and in the home cage until recovery from anesthesia.

A potential limitation to this complex experimental design comparing the effects of a single 'hit', PAE, to a double 'hit', i.e., PAE + Stroke, is that we did not include animals in this study which were subject to a sham stroke surgery which would have included the insertion of a needle intracerebrally in an anesthetized animal. The surgical insertion of a needle into the brain, equivalent to a stab-injury model for traumatic brain injury,[44] possibly constitutes a second hit by itself. To address the possibility that surgery procedure itself could elicit a systemic inflammatory response, a separate cohort of adult male and female rats that were either stroke naïve (6 females, 5 males) or exposed to sham surgery (6 females, 5 males), i.e., anesthesia followed by needle insertion into the brain to the same stereotaxic coordinates as above were assessed. Serum was collected for analysis of inflammatory cytokines, IL-1β, TNF-α and IL-13, 96 hours later. No statistically significant differences were found in systemic pro-inflammatory cytokine levels, between naïve and sham surgery animals (Figure S1).

Neurological score

As we have previously published,[13,14] stroke induced disabilities were assessed by a composite neurological score, equivalent to the National Institutes of Health stroke and Glasgow coma scales in humans, and consistent with the Stroke Treatment Academic Industry Roundtable recommendations,[62] because lesion size does not always correlate with poststroke functional deficits. Briefly, the neurological score was used to assess various behavioral deficits at 48 hours post-MCAo and incorporated 5 different features: (1) forepaw disability, (2) righting reflex, (3) forepaw grip strength, (4) mobility, and (5) circling.

Extraction of tissues and blood Isolation

At 48 hours following MCAo, five month-old PAE and control offspring as well as age-matched stroke-naïve animals from both prenatal exposure groups were anesthetized with xylazine (12.8 mg/kg bwt) and ketamine (88 mg/kg bwt), decapitated and trunk blood collected. Mesenteric adipose, liver, and right and left brain hemispheres were excised and processed either for cytokine quantification or RNA-sequencing. Results of cytokine quantification of plasma, mesenteric adipose, and liver in stroke-naïve animals, are previously published in.[17] Plasma, mesenteric adipose and liver cytokine data from that study were extracted and merged with data from the current study for reanalysis.

Cytokine assays

Brain cytokine/chemokine expression was measured using a multiplexed magnetic bead immunoassay (Millipore Corp. MA) following manufacturer's instructions and our previous protocols.[17] Brain tissues were homogenized in RIPA lysis buffer, centrifuged at 15000g for 15 min at 4 deg C, the supernatant was collected and stored at -20 deg C. Briefly, the 96 well plate was blocked with assay buffer for 10 min and decanted. Standards and samples (100 ug) were added into appropriate wells, followed by addition of premixed beads, and incubated at room temperature for 2h on a plate shaker. Wells were washed twice, 25 μl of detection antibody was added, incubated for 1h and followed by 30 min incubation with 25 μl of streptavidin-phycoerythrin per well. After 2 washes, beads were resuspended in 150 μl of sheath fluid and a minimum of 50 beads per analyte was analyzed in a Bio-Plex suspension array system (Bio-Rad Laboratories, CA). Cytokine/chemokine levels were normalized to total protein content. Total protein was determined using a commercially available colorimetric kit (Pierce BCA protein assay kit, Thermofisher, CA). The following cytokines and chemokines were assessed: Interleukin-1-alpha (IL-1α), IL-4, IL-1β, IL-2, IL-5, IL-6, IL-10, IL-13, IL-17A, IL-12-p-70, interferon-gamma (IFN-γ), monocyte chemoattractant protein-1 (MCP-1), Interferon gamma-induced protein 10 (IP-10), keratinocytes-derived chemokine (KC,) tumor necrosis factor-alpha (TNF-α), Regulated upon Activation, Normal T Cell Expressed and Presumably Secreted (RANTES), macrophage inflammatory protein 1-alpha (MIP1-α), macrophage inflammatory protein 1-beta (MIP1-β), macrophage inflammatory protein 2 (MIP-2), granulocyte colony-stimulating factor (G-CSF), Granulocyte-macrophage colony-stimulating factor (GM-CSF), eotaxin, leptin, epidermal growth factor (EGF), vascular endothelial growth factor (VEGF), fractalkine, lipopolysaccharide-induced CXC chemokine (LIX).

RNA Isolation and RNA Library preparation and sequencing

Total RNA from the mesenteric adipose and liver was isolated using the miRNeasy mini kit (Qiagen; Catalog # 217004). Prior to analysis, RNA quality was assessed using an Agilent TapeStation RNA assay. Total RNA concentration was quantified via Qubit Fluorometric assay, and all samples were normalized to an equivalent starting concentration. Sequencing libraries were prepared using the TruSeq Stranded Total RNA with Ribo-Zero Library Preparation kit (Illumina; San Diego, CA). Each sample was uniquely indexed (barcoded) to allow for the pooling of all samples in a single sequencing run. Library size and quality were then assessed with an Agilent TapeStation D1000 DNA assay. Samples were normalized to ~4nM and pooled equally. Sequencing was performed on an Illumina NovaSeq S4 Flow Cell, XP running with a 150 cycle, paired-end (2x150) sequencing run to generate approximately 50 million read pairs per sample.

Real time PCR was performed on the same samples to validate selected genes that were identified as differentially regulated by paired-end sequencing. The criterion for selecting genes for validation was a $\log_2$ fold-change of >1.0, normalized gene count of >10,000 and p-value <0.0005 by RNAseq analysis. Primer pairs (key resources table) used for qRT-PCR analysis were targeted to the 5'-end of the mRNA transcript, to amplicons that crossed at least one intron, and were validated by thermal stability analysis for the presence of a single amplicon and by Sanger sequencing of amplicons.

QUANTIFICATION AND STATISTICAL ANALYSIS

Raw RNA-sequence data were analyzed to identify significant differences in gene expression between the control vs. PAE treatment groups. All reads were evaluated and trimmed of all adapter sequences and low-quality bases using *Trimmomatic* read trimmer.[45] Using *Trimmomatic* and the corresponding adapter sequences file for Illumina, reads were scanned with a sliding window of 5, cutting when the average quality per base drops below 20, then trimming reads at the beginning and end if base quality drops below 25, and finally dropping reads if the read length is less than 35. Reads were then mapped to the *Rattus Norvegicus* genome assembly (mRatBN7.2, https://www.ncbi.nlm.nih.gov/assembly/GCF-015227675.2/). Read mapping was performed using HISAT2 genomic analysis software platform version 2.1.0.[46] Transcript--wise counts were generated using HTSeq.[47] Differential gene expression tests were then performed using DESeq2 software version 2.1.8.3 following the guidelines recommended by Love and colleagues[48] using a 'treatment' x 'sex' experimental design. A total of 22,103 genes had at least one read count in at least one sample and were processed for differential expression analysis using the regularized logs of normalized gene counts derived from DESeq2. All analyses were performed on the Galaxy instance of the TAMU HPRC (https://hprcgalaxy.tamu.edu/).

The 'R' based *EnhancedVolcano* package[49] was used to construct volcano plots. Pathway analysis was conducted using *ReactomePA*[50] on differentially regulated genes (FDR adjusted p-value < 0.05). *ReactomePA* utilized the KEGG database[51] and the *Pathview* R package[52] to visualize differentially regulated pathways. Weighted gene co-expression network analysis (WGCNA) was conducted using the *WGCNA* R package[63] to construct networks of relatedness and identify eigengenes, or 'hub' genes, from gene expression data.

Statistical analyses were conducted using the GraphPad Prism software, version 9.2.0 for Windows or STATA Base Edition, V18.0. Results are expressed as the mean ± SEM. Multivariate analyses of Variance (MANOVA) used the Pillai's Trace Statistic for small sample sizes. For univariate analyses, the overall group effect was analyzed for significance using two-way ANOVA with Šídák's correction for multiple

comparisons post hoc testing when appropriate (i.e., following a significant group effect or given a significant interaction effect between experimental conditions in two-way ANOVA), to correct for a family-wise error rate. All statistical tests, sample sizes, and post hoc analysis are appropriately reported in the results section. A value of $P < 0.05$ was considered statistically significant, and a value of $0.1 < P < 0.05$ was considered as trending towards significance. For identification of differentially regulated genes (DRGs) in the WGCNA, differentially regulated genes were defined by meeting all three independent criteria: (1) unadjusted p-value<0.05, (2) large effect size (Hedge's g >0.8), and (3) nonoverlapping 95% confidence intervals.